Electrochimica Acta 54 (2008) 698–705

Contents lists available at ScienceDirect

Electrochimica Acta

journal homepage: www.elsevier.com/locate/electacta

An alkaline microfluidic fuel cell based on formate and hypochlorite bleach

Erik Kjeang[a,c], Raphaelle Michel[a,c], David A. Harrington[b,c], David Sinton[a,c,*], Ned Djilali[a,c]

[a] Department of Mechanical Engineering, University of Victoria, 3800 Finnerty Road, Victoria, BC V8W 2Y2, Canada
[b] Department of Chemistry, University of Victoria, 3800 Finnerty Road, Victoria, BC V8W 2Y2, Canada
[c] Institute for Integrated Energy Systems (IESVic), University of Victoria, 3800 Finnerty Road, Victoria, BC V8W 2Y2, Canada

ARTICLE INFO

Article history:
Received 5 February 2008
Received in revised form 30 June 2008
Accepted 1 July 2008
Available online 12 July 2008

Keywords:
Microfluidic fuel cell
Alkaline fuel cell
Formate
Hypochlorite bleach
Flow-through porous electrode

ABSTRACT

An alkaline microfluidic fuel cell is demonstrated employing an alkaline version of a formic acid anode and a sodium hypochlorite cathode. Both sodium formate fuel and sodium hypochlorite oxidant are available and stable as highly concentrated solutions, thereby facilitating fuel cell systems with high overall energy density. Sodium hypochlorite is commonly available as hypochlorite bleach. The alkaline anodic half-cell produces carbonate rather than the less-desirable gaseous CO_2, while sustaining the rapid kinetics associated with formic acid oxidation in acidic media. Both half-cells provide high current densities at relatively low overpotentials and are free of gaseous products that may otherwise limit microfluidic fuel cell performance. The microfluidic fuel cell takes advantage of a recently developed membraneless architecture with flow-through porous electrodes. Power densities up to 52 mW cm^{-2} and overall energy conversion efficiencies up to 30% per single pass are demonstrated at room temperature using 1.2 M formate fuel and 0.67 M hypochlorite oxidant. The alkaline formate/hypochlorite fuel and oxidant combination demonstrated here, or either one of its individual half-cells, may also be useful in conventional membrane-based fuel cell designs.

1. Introduction

A microfluidic fuel cell is defined as a device that incorporates all fundamental components of a fuel cell within a single microfluidic channel and its walls. Since its invention in 2002, microfluidic fuel cell technology has developed rapidly [1–22] and is now considered a candidate for commercial small-scale portable power generation. Microfluidic fuel cells typically operate without a membrane, and the most common configurations rely on the laminar nature of flow in microstructures to maintain sufficient separation of fuel and oxidant streams, flowing side-by-side in a co-laminar format. Supporting electrolyte contained in both co-laminar streams facilitates ionic conduction between the electrodes. Mixing by diffusion is restricted to an interfacial width at the center of the channel, depending on mean velocity and channel geometry. The electrode spacing is typically an order of magnitude larger than the interdiffusion width. Microfluidic fuel cells have several advantages as compared to traditional proton exchange membrane (PEM)-based fuel cells: fuel and oxidant streams may be combined in a single microchannel; fuel and/or oxidant crossover can be mitigated by adjusting the flow rate of the co-laminar streams; no ion exchange membrane is required; sealing, manifolding, and fluid delivery infrastructure requirements are reduced; and issues related to membrane hydration and water management are eliminated. In addition, microfluidic fuel cells may be manufactured using inexpensive microfabrication methods and low-cost materials.

Microfluidic fuel cells with room-temperature power densities on the order of 100 mW cm^{-2} have been demonstrated [15,16]. Operation at high power densities has, however, resulted in low overall energy conversion efficiency due to low single-pass fuel utilization. To mitigate this problem, a new microfluidic fuel cell architecture with flow-through porous electrodes was recently developed by our group [15]. The flow-through design is based on cross-flow of reactant through the porous electrodes into a co-laminar center channel with orthogonally directed flow in which the waste solutions facilitate ionic charge transfer in a membraneless configuration. This cell architecture enables improved utilization of the three-dimensional active area inside the porous electrodes and provides enhanced rates of convective/diffusive transport to the active sites without increasing the parasitic loss required to drive the flow. When operated with 2 M vanadium solutions, the flow-through design demonstrated a high level of overall energy conversion efficiency, as a relatively high level of fuel utilization and cell voltage were achieved concurrently. With respect

* Corresponding author at: Department of Mechanical Engineering, and the Institute for Integrated Energy Systems (IESVic), University of Victoria, 3800 Finnerty Road, Victoria, V8W 2Y2, Canada.
E-mail address: dsinton@me.uvic.ca (D. Sinton).

0013-4686/$ – see front matter © 2008 Elsevier Ltd. All rights reserved.
doi:10.1016/j.electacta.2008.07.009

to overall energy density, the solubility and concentration of ions is a limitation of microfluidic fuel cell systems based on vanadium redox species; in addition, the associated redox reactions provide only one electron per ion.

In the context of fuel and oxidant combinations for microfluidic fuel cell systems with practical energy density, the following attributes are desirable: both reactants and products are available and stable at high concentration in the liquid phase; the reactants provide at least two electrons per molecule; spontaneous and/or electrochemically activated decomposition into gaseous products are prevented; the fuel and oxidant do not react upon mixing; and if the anodic and cathodic supporting electrolytes are different, both fuel and oxidant species are stable in both electrolytes.

Several different fuels have been employed in microfluidic fuel cells presented to date. These include hydrogen [7,18,19], methanol [5,6,11], formic acid [4,8,12,13], vanadium redox species [9,14–16], and hydrogen peroxide [10]. Most liquid hydrocarbon fuels produce carbon dioxide (CO_2) as the end product after complete electrochemical conversion. Typically, CO_2 evolves as a gaseous product in acidic or neutral media [13] unless the current densities are low enough to fully dissolve it in the fuel or electrolyte stream [4]. Formic acid is an established fuel with high energy density that has previously been used in both PEM-based direct formic acid fuel cells [23,24] and microfluidic fuel cells [4,8,12,13], and its electrochemical kinetics on palladium catalyst are fast, thereby allowing much higher power densities than other hydrocarbon fuels such as methanol [25]. In contrast to acidic and neutral media, alkaline media have the capability of absorbing large amounts of CO_2 as carbonates with the additional benefit of automated carbon sequestration. An alkaline formate fuel from concentrated formic acid therefore accomplishes all the criteria for an all-liquid microfluidic fuel cell system with high energy density.

The oxidants employed in microfluidic fuel cells to date have been oxygen [4–8,18,19], air [11,12], vanadium redox species [9,14–16], and hydrogen peroxide [10,13]. Among these, only hydrogen peroxide is available as a highly concentrated liquid. Direct hydrogen peroxide reduction on common catalysts such as platinum and palladium is however frequently accompanied by oxygen gas evolution from its decomposition [13]. Alternative liquid oxidants that have been employed in fuel cells or flow batteries include permanganate [4,26] and hypochlorite [27,28]. Permanganate is a strong oxidant that enables high current densities and highly positive reduction potentials in acidic media [29]. Reports have shown, however, that product manganese dioxide precipitate can clog the pores of a microporous electrode in the absence of stirring [26]. The use of permanganate oxidant in microfluidic fuel cells that incorporate both microporous electrodes and microscale channels should therefore be avoided. Hypochlorite, in contrast, does not produce any precipitate, and has shown benign electrochemical characteristics as an oxidant in magnesium, zinc and aluminum semi-fuel cells [27,28] using palladium/iridium and platinum catalysts. Hypochlorite oxidant has many useful characteristics for microfluidic fuel cell implementation: relatively high standard reduction potential and rapid kinetics; high solubility in aqueous media; highly soluble reduction product (chloride); and finally, no gaseous decomposition reactions take place when the hypochlorite is used in an alkaline electrolyte [27]. Furthermore, hypochlorite solution is produced in large quantities as domestic bleach. Sodium hypochlorite bleach is considered relatively safe and is available at very low cost. Hypochlorite therefore meets all the criteria of an all-liquid microfluidic fuel cell with high energy density. Additionally, the product sodium chloride is common and non-toxic.

In this work, a microfluidic fuel cell based on alkaline formate and hypochlorite bleach is presented. Both palladium and gold porous electrodes are formed via electrodeposition on a porous carbon substrate. The electrochemical responses of the porous electrodes are characterized in a stationary three-electrode cell prior to *in situ* tests and fuel cell implementation.

2. Experimental

2.1. Preparation of solutions

Alkaline formate fuel solution was obtained by adding 5 wt.% concentrated formic acid (HCOOH; Fisher Sci., Fair Lawn, NJ) to a 10 wt.% (2.8 M) sodium hydroxide (NaOH) electrolyte prepared by dissolving NaOH pellets (EMD Chemicals, San Diego, CA) in Millipore Milli-Q water (Millipore, Billerica, MA). The resulting solution contained 1.2 M formate and 1.6 M OH^-. Alkaline hypochlorite (ClO^-) oxidant solution (0.67 M) was prepared by dissolving 10 wt.% (2.8 M) NaOH pellets directly in a 5% sodium hypochlorite solution (NaOCl; Caledon, Georgetown, Canada) or 5.25% hypochlorite bleach (Javex-5; Colgate-Palmolive, Toronto, Canada). The gold (Au) plating solution consisted of 17 mM potassium gold cyanide ($KAu(CN)_2$; Degussa, Frankfurt, Germany) dissolved in Millipore Milli-Q water, followed by the successive addition of 0.4 M citric acid ($C_6H_8O_7$; Matheson Coleman & Bell, Montreal, Canada) and 0.4 M sodium citrate ($Na_3C_6H_5O_7$; Merck, Montreal, Canada) to a final pH of 3–5. The palladium (Pd) plating solution consisted of 1.0 wt.% palladium(II) chloride ($PdCl_2$; Sigma–Aldrich) in 1 M hydrochloric acid (HCl; Anachemia, Montreal, Canada) in Millipore Milli-Q water. All chemicals used were ACS grade except the hypochlorite bleach.

2.2. Electrodeposition

Porous carbon electrodes subject to catalyst deposition were cut to 25 mm × 1 mm strips from sheets of Toray carbon paper (B-2 Designation TGPH-090; E-TEK, Somerset, NJ) with typical thickness 300 μm (measured), typical density 0.49 g cm^{-3} and 78% porosity. A 20 mm long section of the carbon strips were rendered hydrophilic by annealing (~1 s) in a propane flame, and the hydrophilic electrodes were then supported on glass slides with wires attached using PELCO® conductive silver 187 (Ted Pella Inc., Redding, CA) covered by regular epoxy. The strip electrodes were rinsed thoroughly in Millipore Milli-Q water before and after each plating sequence. Electrodeposition of Au and Pd on the porous carbon electrodes was performed by immersing the hydrophilic electrode parts in a bath containing either Au or Pd plating solution, together with a Pt mesh counter electrode and a saturated calomel reference electrode (SCE). The carbon working electrode was aligned with the counter electrode to obtain a uniform current distribution during plating. All electrochemical experiments in this study were driven by a PARSTAT 2263 potentiostat (Princeton Applied Research, Oak Ridge, TN), and all individual electrode potentials are given versus the SCE (sat. KCl) reference electrode (0.241 V vs. SHE). Each electrodeposition experiment started with a cyclic voltammogram (3 cycles) of a bare porous carbon electrode in the Au plating solution from the open-circuit potential (OCP) to −1.1 V, followed by electroplating under potentiostatic control at −1.1 V for 60 min. The Au loading of the obtained porous gold electrodes was not assessed. Porous Pd electrodes were obtained by electrodeposition of Pd on the fresh Au layer by a similar procedure [13]: a cyclic voltammogram (3 cycles) was measured with the porous Au electrode in the Pd plating solution from the OCP to −0.1 V, followed by electroplating under potentiostatic control at 0.0 V until a desired loading of 5 mg cm^{-2} had been deposited, typically after 20–30 min, calculated in real time by integrating the current profile and assuming a 60% coulombic plating efficiency [30]. Scanning

electron micrographs were captured by a Hitachi S-3500N scanning electron microscope with a tungsten filament operated at 15 kV.

2.3. Fuel cell fabrication

A collection of microfluidic fuel cells with flow-through porous electrodes was assembled using in-house developed microfabrication techniques detailed in a previous study [15]. In short, one 20 mm long porous Pd anode and one 20 mm long porous Au cathode were cut from the electrodeposited strip electrodes and fitted in custom-sized grooves (20 mm × 1 mm × 300 μm, separated by 1 mm), fabricated in a poly(dimethylsiloxane) (PDMS; Dow Corning, Midland, MI) part. Of the 20 mm length of electrode, only 12 mm was exposed to the solutions; the remaining 8 mm allowed for electrical contact and sufficient separation between the contact and the electrolyte. The PDMS part had a dual layer structure: a 300 μm deep section that defined the two electrode grooves plus the two inlet channel structures, and a 150 μm deep layer accommodating the co-laminar flow channel between the electrodes, leading towards the outlet. The fourth wall of the microfluidic device was provided by a flat layer of PDMS, with previously punched holes for the inlets, outlet, and electrical contacts, which was sealed irreversibly on top of the other PDMS part after plasma-treating. External wiring was contacted to the exposed ends of the carbon strip electrodes using PELCO® conductive silver 187 covered with regular epoxy.

2.4. Fuel cell testing

The co-laminar flow of formate and hypochlorite solutions through the fuel cell was driven by a syringe pump (PHD 2000; Harvard Apparatus, Holliston, MA) via Teflon® tubing (1/16 in. diameter; S.P.E. Limited, North York, ON, Canada) to the inlets and through a larger Tygon® tube (3 mm diameter; Fisher Sci., Pittsburgh, PA) from the outlet to the outlet reservoir. The desired flow rate was adjusted and the co-laminar flow was stabilized before initiation of the electrochemical measurements. Cell polarization data were measured by chronoamperometry under stepwise potentiostatic control from the open-circuit cell voltage down to 0.0 V by −0.2 V increments, using the PARSTAT potentiostat. The current transient generated by the cell was monitored until steady state was reached, which typically occurred within 180 s. Polarization of individual electrodes was measured versus an external SCE reference electrode placed in the outlet reservoir, using the opposite fuel cell electrode as counter electrode.

The definition of an area with which to characterize the performance of flow-through cells is somewhat ambiguous due to the three-dimensional architecture. The porous electrodes employed here were 1 mm wide, 300 μm deep, and a length of 12 mm was exposed to the solutions. Utilization of the high internal surface area (estimated at 3 cm^2) is a feature of this fuel cell architecture. To make meaningful performance comparison with previous microfluidic fuel cells, however, current densities and power densities reported here were calculated based on the vertically projected area of the electrodes (1 mm × 12 mm = 0.12 cm^2). This is the geometric area in the fluidic plane of the fuel cell, and is significantly larger than the geometric area in the flow-normal direction. As noted previously [15], power-per-volume, while unconventional, is ultimately a more pertinent performance metric from a device perspective.

The ohmic resistance of the fuel cell and its individual electrodes was measured by electrochemical impedance spectroscopy (EIS), using the PARSTAT 2263 potentiostat. Impedance spectra were recorded at the open-circuit cell voltage, by applying an ac amplitude of 5 mV rms over the frequency range from 50 kHz to 0.5 Hz with 30 log spaced data points. The ohmic resistance was calculated as the high-frequency real axis intercept of the Nyquist plot of impedance. For *in situ* EIS measurements, the flow rate was fixed at 60 μL min^{-1}.

3. Results and discussion

3.1. Reaction scheme

At the pH used here, the fuel exists predominantly as formate ($HCOO^-$), the oxidant as hypochlorite (ClO^-) and the CO_2 as carbonate. The reactions, written in terms of these species, lead to the following standard electrode potentials (vs. SCE) at 298 K ((1) calculated from Gibbs' energies of formation in [31] and (2) taken from [32]):

Anode:

$$HCOO^- + 3OH^- \rightleftharpoons {CO_3}^{2-} + 2H_2O + 2e^-, \quad E^0 = -1.17\,V \tag{1}$$

Cathode:

$$ClO^- + H_2O + 2e^- \rightleftharpoons Cl^- + 2OH^-, \quad E^0 = 0.57\,V \tag{2}$$

Overall cell reaction:

$$HCOO^- + ClO^- + OH^- \rightleftharpoons {CO_3}^{2-} + Cl^- + H_2O, \quad E^0_{cell} = 1.74\,V \tag{3}$$

Note that the actual half-cell and cell reversible potentials also depend on pH and concentration of the aqueous species according to the Nernst equation. The cell reaction involves some net consumption of OH^-, which is available at high concentration in the alkaline electrolyte.

3.2. Electrodeposition of porous electrodes

To reduce the activation overpotentials of the proposed electrochemical reaction scheme, suitable catalysts need to be added to the electrodes. In this study, palladium (Pd) and gold (Au) were selected as the catalysts for formate oxidation and hypochlorite reduction, respectively. Pd and Au were electrodeposited on porous carbon paper substrates in order to develop porous Pd and Au electrodes compatible with the unique co-laminar flow mechanism of the microfluidic fuel cell with flow-through porous electrodes [15]. Coating of the carbon fibers with Au may also be advantageous towards reducing the overall ohmic resistance of the electrodes, which was relatively high for the bare porous carbon electrodes used previously with this cell architecture [15]. Fig. 1a shows a typical cyclic voltammogram of a bare porous carbon electrode in the gold cyanide plating bath. The overpotential for Au plating is relatively high; plating effectively started at −0.6 V, which was about 800 mV negative of the open-circuit potential (OCP). Hydrogen evolution started at about −1.0 V on the first scan and at −0.8 V on consecutive scans. The difference between the three cycles is associated with the fresh Au deposit on the carbon electrode that reduced the overpotential for hydrogen evolution, which is relatively high on bare carbon. Au plating below −0.8 V was therefore accompanied by hydrogen evolution. The viability of potentiostatic Au plating on porous electrodes was evaluated at three different potentials: −0.7 V, −0.9 V and −1.1 V, with results shown in Fig. 1b. The plating current at −0.7 V was essentially free from hydrogen evolution and therefore quite low. Although not readily apparent on the scale of the plot in Fig. 1b, the current showed a linear increase from 0.15 to 0.45 mA/cm^2 (over the 1 h test period), attributed to the nucleation and growth of Au grains. The plating currents measured at −0.9 V and −1.1 V were dominated by hydrogen evolution, which also increased over time as the surface area of the Au deposit

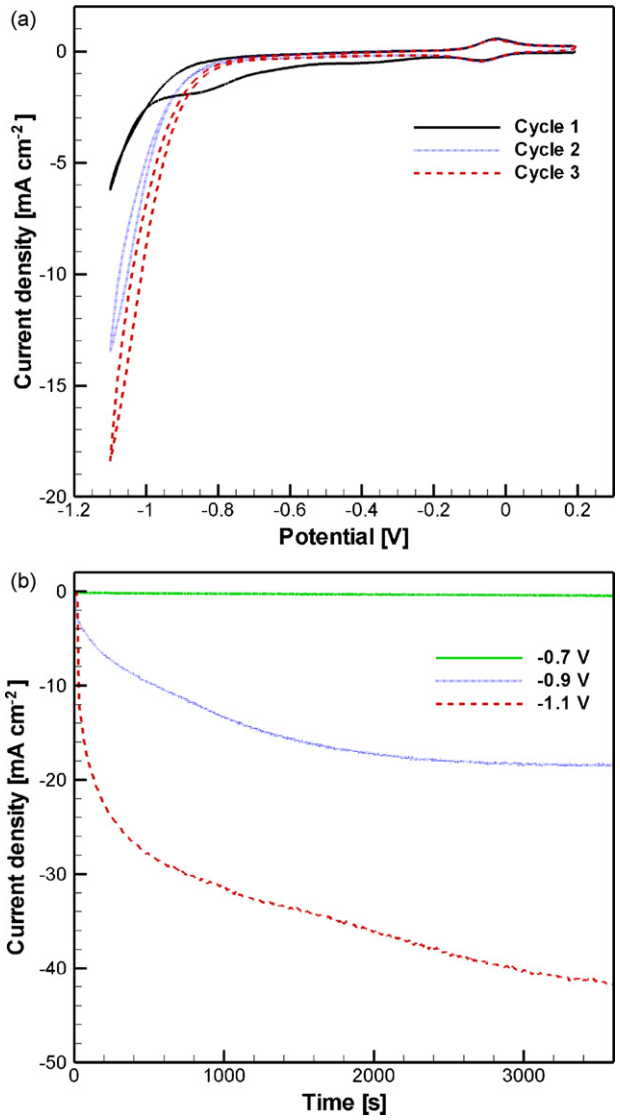

Fig. 1. Electrodeposition of gold on porous carbon electrodes: (a) cyclic voltammogram of a bare substrate in gold cyanide plating solution measured at 50 mV s^{-1}, and (b) potentiostatic deposition curves of 1 h duration at three different potentials (as indicated vs. SCE).

was enlarged. Images of the final Au deposits captured by scanning electron microscopy (SEM) are presented in Fig. 2. These images provide a useful illustration of the microstructure and degree of coverage achieved in the deposition of Au on the porous carbon electrodes. With respect to the electrochemical performance of a porous electrode, both high coverage and high specific surface area are desirable characteristics. Fig. 2a shows the granular Au structure obtained at −0.7 V. At −0.9 V (Fig. 2b), a similar granular structure was observed with significantly higher loading. The image of the deposit obtained at −1.1 V (Fig. 2c) indicates a high degree of coverage with different surface morphology. Most importantly, the Au deposit appeared much more uniform over the observable depth of the porous electrode at −1.1 V compared to the other potentials.

The porous Au electrode deposited at −1.1 V was further analyzed with images obtained at three different magnifications, shown in Fig. 3. These images demonstrate the quality of the obtained Au deposit in the context of fuel cell implementation: the outer surfaces of the electrode were uniformly coated (Fig. 3a); all observable fibers throughout the 3-D porous matrix showed effectively complete coverage (Fig. 3b); and the surface morphology had dendritic features with size <1 μm indicating a high specific surface area (Fig. 3c). The improved 3-D coverage at high overpotentials is attributed to the continuous hydrogen gas evolution introducing a local two-phase flow component. Specifically, as hydrogen bubbles were released from the porous matrix, fresh plating solution was introduced into the matrix. Although not evaluated here, convection-assisted plating by stirring or ultrasonic vibration is expected to have a similar effect. In sum, electrodeposition of Au on porous carbon electrodes was shown to be very effective at −1.1 V.

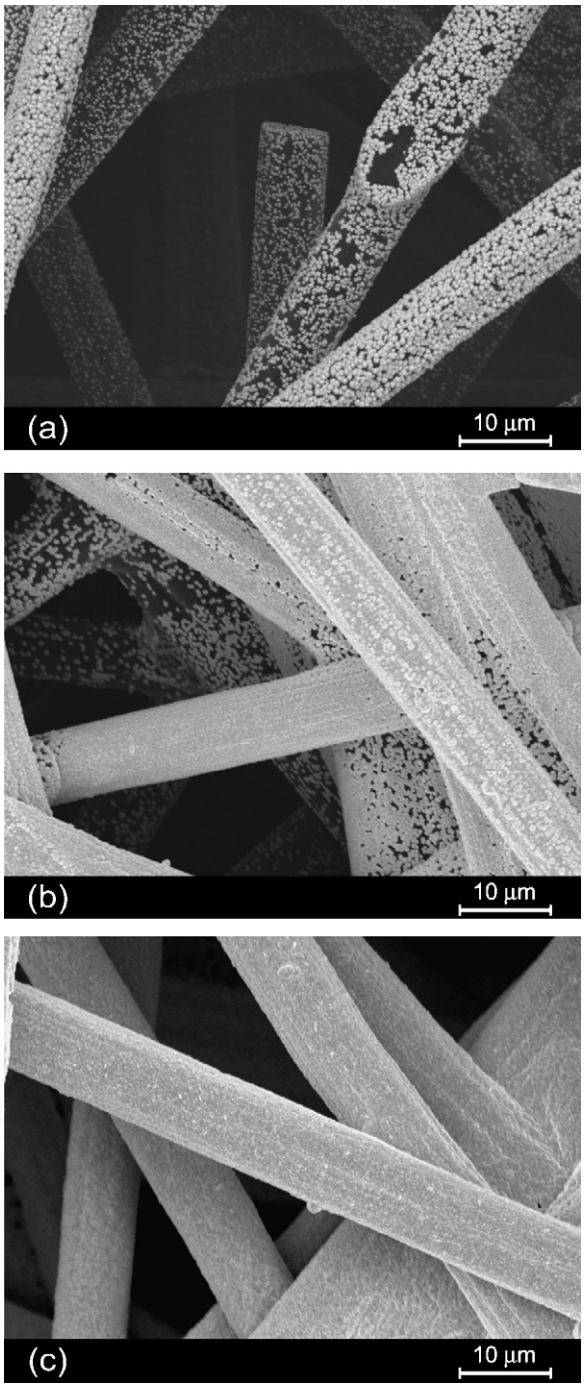

Fig. 2. Scanning electron micrographs showing the microstructure of the porous gold electrodes electrodeposited on carbon paper substrates at (a) −0.7 V, (b) −0.9 V and (c) −1.1 V (SCE), captured at 2000× magnification.

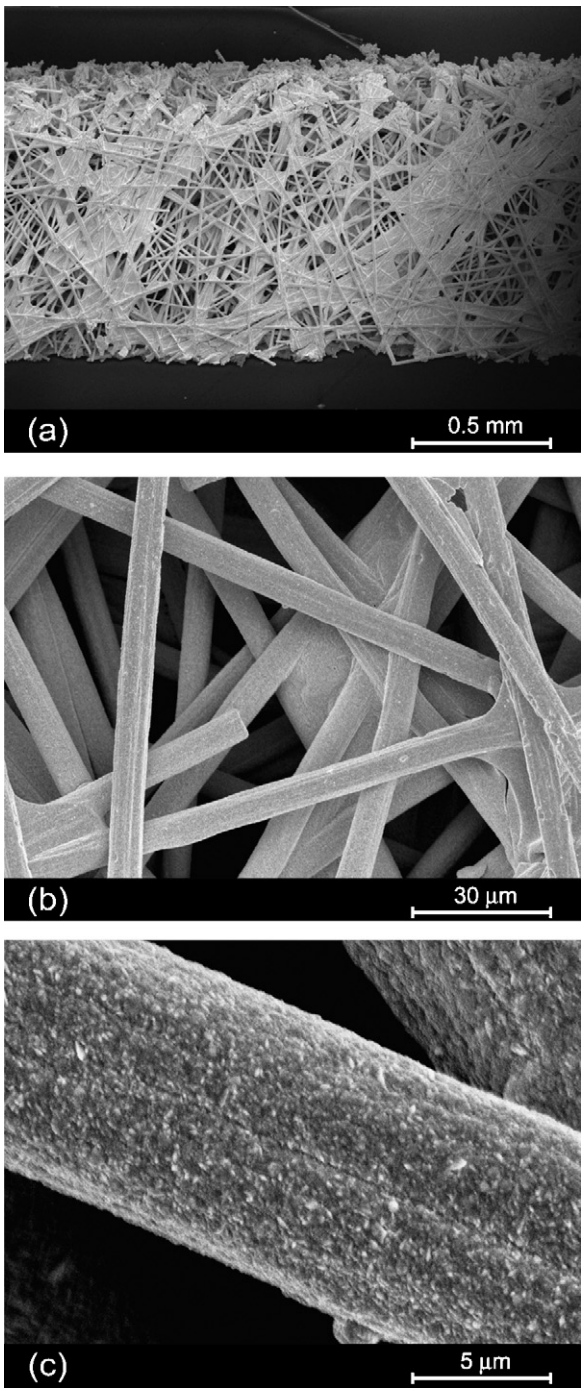

Fig. 3. Scanning electron micrographs of a porous gold electrode electrodeposited at −1.1 V (SCE), captured at (a) 60×, (b) 800× and (c) 6000× magnification.

Similarly fabricated porous Au electrodes were also used to make porous Pd electrodes, by coating an additional Pd layer (5 mg cm^{-2}) following our previously described Pd electrodeposition methodology [13], with details outlined in Section 3.2.

3.3. *Ex situ half-cell characterizations*

The porous Pd anodes and Au cathodes were characterized electrochemically in a stationary three-electrode electrochemical cell in the alkaline formate or hypochlorite solutions, respectively, to analyze their performance and suitability for microfluidic fuel cell implementation. Cyclic voltammograms measured *ex situ* for a porous Pd anode, a porous Au cathode, and a porous Pd cathode are shown in Fig. 4. The Pd anode produced high current densities up to 340 mA cm^{-2} at quite low overpotentials, in the absence of convective motion. As expected, no gas evolution was observed in this anodic half-cell, indicating that the product is carbonate, without any CO_2. The OCP of this half-cell was measured to −0.99 V, within 0.2 V of the standard potential of reaction (1). (The reversible potential cannot be calculated because the product concentrations are unknown.) The ohmic resistance of the Pd anode was measured as 3.6 Ω by electrochemical impedance spectroscopy (EIS), as described in Section 3.4.

The Au and Pd cathodes also delivered notably high current densities up to 230 and 330 mA cm^{-2}, respectively, despite the lack of convective transport. The Au cathode, however, exhibited a 250 mV higher overpotential than the Pd cathode for the hypochlorite reduction reaction (2). As shown, Au is not an ideal catalyst for hypochlorite reduction, but it does have a significant advantage with respect to integration in microfluidic fuel cells: in contrast to the Pd electrode that produced a small amount of gas during these tests, no gas evolution was observed on the Au electrode. The OCPs for hypochlorite reduction were measured as 0.38 V (Au) and 0.46 V (Pd). The oxidation of water to oxygen can occur above 0.38 V at pH 14.4, the nominal pH of this solution, explaining the gas evolution in the case of Pd. The measured OCP was again within 0.2 V of the standard reduction potential (0.57 V). While not ideal for catalysis of this reaction, the alkaline electrolyte is required to stabilize the hypochlorite ion in solution. The ohmic resistance of the cathodes was measured by EIS as 3.0 Ω (Au) and 2.9 Ω (Pd). The electrical resistance of the Au coated electrodes was thus reduced by more than 50% compared to the bare carbon strip electrodes (7–9 Ω). Overall, these half-cell experiments indicate that the formate anodic half-cell and the hypochlorite cathodic half-cell are well-suited to implementation in a fuel cell.

An additional half-cell test was performed with the ACS-grade hypochlorite solution replaced with a low-cost household bleach product (Javex-5; Colgate-Palmolive), containing 5.25% sodium hypochlorite. The obtained cyclic voltammograms closely matched those in Fig. 4.

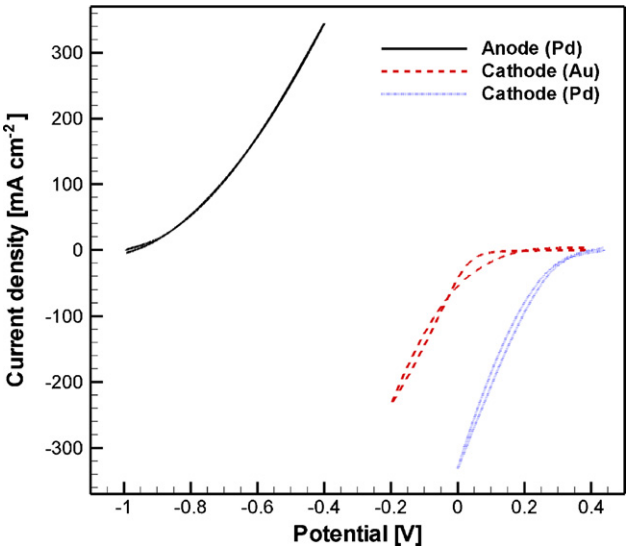

Fig. 4. Cyclic voltammograms measured ex situ for formate oxidation on a porous palladium anode and hypochlorite reduction on porous gold and palladium cathodes in a stationary three-electrode electrochemical cell. The anolyte and catholyte consisted of 1.2 M formate and 0.67 M hypochlorite, respectively, in alkaline solution. The scan rate was 50 mV s^{-1}.

3.4. Microfluidic fuel cell implementation

A microfluidic fuel cell with flow-through porous electrode architecture was fabricated, incorporating an electrodeposited porous Au electrode as cathode and an electrodeposited porous Pd/Au electrode as anode. A schematic of the microfluidic fuel cell architecture is given in Fig. 5a, and the assembled cell is shown in Fig. 5b and c. The transparency of the PDMS enables observation of the flow, and detection of any intermittent disturbances. As gaseous products can destabilize the co-laminar flow [13], the Au cathode was chosen over the Pd cathode (that produced a small amount of gas in the *ex situ* experiments) for implementation in the fuel cell. The fuel and oxidant streams enter the microfluidic fuel cell device (Fig. 5) through separate inlets and approach the electrodes via the deep (300 μm) distribution channels. From the distribution channels, the flow is directed orthogonally into the porous electrodes. The cross-flow through the porous media has two orders of magnitude higher pressure drop than the flow in the distribution channels [15], and is therefore expected to be uniformly distributed throughout the available cross-sectional area of the electrodes. In addition, the high cross-sectional area open to the cross-flow provides low mean velocities inside the porous electrodes, which enables ample opportunity for high coulombic fuel utilization. Both anodic and cathodic streams enter the center channel through the electrodes on both sides at the same flow rate. The two streams are directed towards the outlet in a co-laminar format. The center channel is relatively shallow (150 μm) and has a small cross-sectional area in order to provide high mean velocities and reliable co-laminar flow. In this way mixing of the waste streams is limited to a relatively small diffusion width in the centre, while the electrolyte provides effective ionic transport. The flow-through electrode architecture thus achieves utilization of the full depth of the electrode and associated active area, which is 20–30 times larger than the vertically projected area of the electrode [16], and provides enhanced species transport from the bulk to the active sites as well as effective ionic transport in a membraneless configuration.

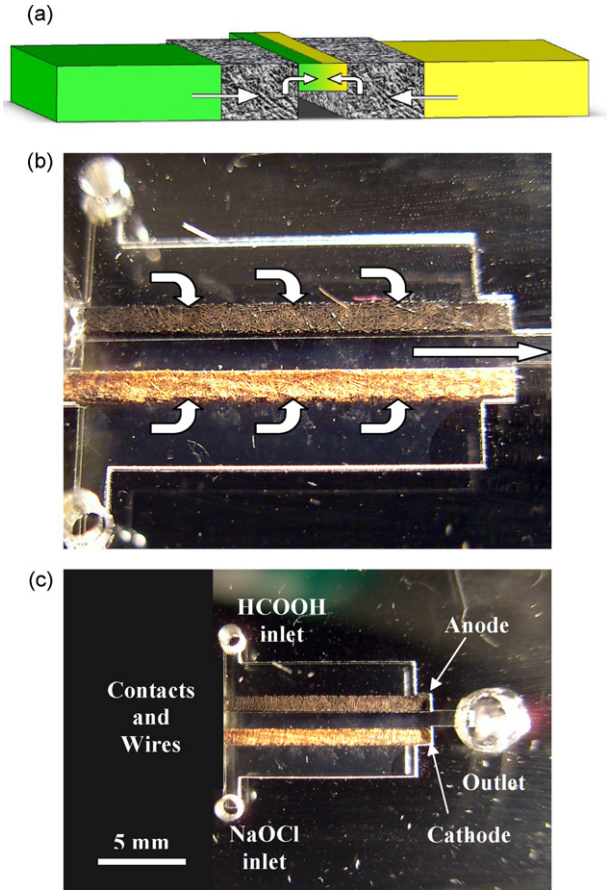

Fig. 5. The microfluidic fuel cell with flow-through porous electrodes: (a) schematic of the fuel cell architecture in cross-section; (b) image of the assembled fuel cell with porous palladium and gold electrodes with microchannel flow arrows superimposed; and (c) labeled image of the assembled cell.

Table 1
Selected resistances measured by electrochemical impedance spectroscopy (EIS): *ex situ* electrode resistances measured in a stationary three-electrode electrochemical cell, and *in situ* electrode and cell resistances measured in the fuel cell assembly during operation at 60 μL min^{-1} flow rate

Resistance [Ω]	*Ex situ*	*In situ*
Anode (Pd)	3.6	7.0
Cathode (Au)	3.0	12.8
Cell	–	24.1

3.5. Microfluidic fuel cell performance

The assembled microfluidic fuel cell device with flow-through porous electrodes was operated at flow rates ranging from 2 to 300 μL min^{-1} per stream, using formate anolyte and hypochlorite catholyte. The cell exhibited very stable co-laminar flow without any gas evolution or other disturbances and the open-circuit cell potential was steady between 1.37 and 1.42 V. The OCP increased somewhat with flow rate, perhaps because the OCP at the cathode is a mixed potential with a component of oxygen evolution and is more easily perturbed than a true reversible potential. These cell potential levels are similar to the estimated cell potential from the *ex situ* experiments (1.37 V), calculated as the difference in OCP between the Pd anode and the Au cathode. The combined ohmic resistance of the cell was measured using EIS at open circuit and 60 μL min^{-1} as 24.1 Ω. This resistance measurement includes the solution resistance with respect to ionic transport in the co-laminar center channel and the electrical resistance in electrodes, contacts and wires. By incorporation of an external reference electrode (SCE) in the outlet reservoir, we were also able to measure the ohmic resistance of the individual electrodes *in situ* using the same technique, resulting in 7.0 Ω for the anode and 12.8 Ω for the cathode. A summary of the resistance measurements is provided in Table 1. The *in situ* values are somewhat higher than the corresponding *ex situ* measurements (3.6 Ω and 3.0 Ω, respectively), primarily attributed to high electrical contact resistance on the chip. The solution resistance was estimated to 4.3 Ω by subtracting the electrical resistance from the combined ohmic cell resistance, which is in agreement with previous studies using acidic electrolyte [14].

Room-temperature polarization data were obtained under potentiostatic control at steady state conditions. Fig. 6 presents three different polarization curves obtained at 2, 10 and 60 μL min^{-1}. The current densities increased with flow rate up to a maximum 230 mA cm^{-2} at 60 μL min^{-1}, indicating partial mass transport control and relatively fast electrochemical kinetics; however, increasing the flow rate above 60 μL min^{-1} (polarization curves not shown here) resulted in no significant performance improvements. Based on these observations, electrochemical kinetics and ohmic resistance were dominating at high flow rates. The parasitic combined ohmic resistance of the cell contributed almost 50% to the average slope of the polarization curve (51 Ω) at 60 μL min^{-1}, and about 70% to the linear part of the curve at practical cell voltages of 0.8 V and below. At low flow rates, the potential loss associated with ohmic resistance was not as severe: it was less than 30% at 10 μL min^{-1} and only about 8% at 2 μL min^{-1}. At these

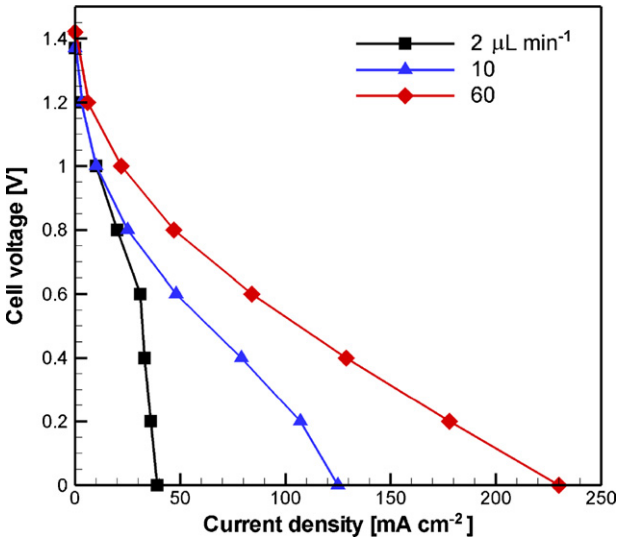

Fig. 6. Fuel cell polarization curves measured experimentally at steady state and room temperature, for operation of the formate/hypochlorite microfluidic fuel cell at three different flow rates (as indicated).

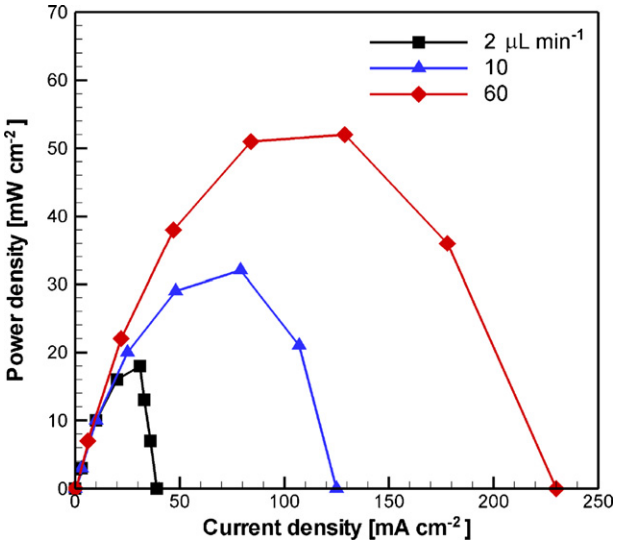

Fig. 8. Power density curves for formate/hypochlorite fuel cell operation at steady state and room temperature, measured at three different flow rates (as indicated).

flow rates, the current densities were primarily controlled by the rate of reactant supply. The cell was not operated below 2 μL min^{-1}, although the stability of the co-laminar flow is expected to be maintained at least down to 0.3 μL min^{-1} [15].

The relatively low current densities produced in the high cell voltage range (1.0–1.4 V) indicate significant activation overpotential for the electrochemical reactions, which is common to most fuel cell systems. This effect was further analyzed by employing the external reference electrode (SCE) to measure the performance of the individual electrodes *in situ* under the same flow conditions, using the opposite electrode as counter electrode. Separate anodic and cathodic polarization curves are presented in Fig. 7. This type of analysis is often used to diagnose overall fuel cell performance and to identify half-cell-specific limitations. Given the significant differences related to the electrochemistry of the formate oxidation and hypochlorite reduction reactions, the anodic and cathodic polarization curves are surprisingly well-balanced. The symmetry outlined by the two curves justifies the viability of the formate/hypochlorite fuel and oxidant combination and also confirms the uniform transport characteristics of the flow-through architecture. Both electrodes responded well to fuel cell operation at cell voltages below 1.0 V, where neither of them caused an overall restriction to the cell. The activation overpotential was shared by the two half-cells but dominated by the cathode. These results are in good agreement with the *ex situ* measurements, where the activation overpotential was quite high on the Au cathode. The flow-through fuel cell architecture was endurance tested previously [15]. The performance over 10 h was very stable, with no observable loss in performance over that period. Similarly the alkaline cell tested here showed no detectable degradation over the course of this study.

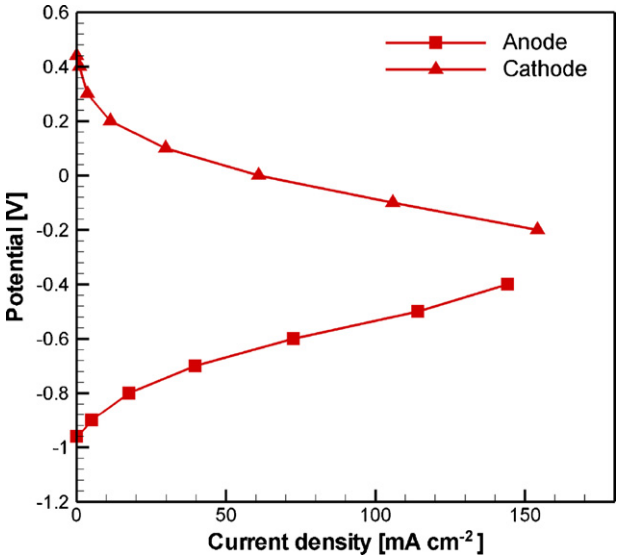

Fig. 7. Fuel cell polarization data of anode and cathode measured *in situ* at room temperature and 60 μL min^{-1} flow rate, using the opposite fuel cell electrode as counter electrode and an external reference electrode (SCE).

Power density curves calculated based on the polarization data at 2, 10 and 60 μL min^{-1} are provided in Fig. 8. The overall power density increased significantly with flow rate, which again confirms the partial mass transport control. The highest power density measured in this study was 52 mW cm^{-2} at 0.4 V and 60 μL min^{-1}. This level of power density compares favorably to most other microfluidic fuel cells reported to date and demonstrates the high capacity of the proposed formate/hypochlorite fuel and oxidant combination. The power densities measured here did not however reach the levels obtained with the vanadium redox system in the same cell architecture [15] due to the lower cell voltages and reactant concentrations. The feasibility of the formate/hypochlorite system in the flow-through electrode architecture is more evident in the low flow rate regime. Even at the lowest flow rate (2 μL min^{-1}), a useful peak power density of 18 mW cm^{-2} was generated at 0.6 V cell voltage. Fuel cell operation in this regime is very efficient due to the high levels of fuel utilization enabled by the flow-through electrode architecture and practical cell voltages achieved concurrently. The fuel utilization with respect to the hypochlorite component, which had a lower molar concentration (0.67 M) than the formate solution (1.2 M), was as high as 85% at the point of peak power and effectively 100% at low cell voltages. Based on the theoretical standard cell potential of 1.74 V, the overall energy conversion efficiency at 0.6 V was ~30% per single pass. The highly energy efficient microfluidic fuel cell performance previously demonstrated with the vanadium redox

system was thus maintained with the new formate/hypochlorite system.

The fuel cell performance measured here can also be compared to the *ex situ* half-cell characterizations provided by the cyclic voltammograms in Fig. 4. In contrast to the steady state fuel cell data, these predictions are based on unsteady operation (50 mV s^{-1} scan rate) without flow, and the ohmic resistance was only about 3 Ω per electrode. A fuel cell based on the performance measured in the *ex situ* experiments would theoretically have an open-circuit voltage of 1.37 V (Au cathode) or 1.45 V (Pd cathode), and would produce peak power densities of 81 mW cm^{-2} (Au cathode) and 143 mW cm^{-2} (Pd cathode) at 0.35 V and 0.55 V cell voltage, respectively. These power density levels are much higher than those obtained in the microfluidic fuel cell, despite the lack of convective transport. This comparison indicates that the high capacity inherent to the formate/hypochlorite system was not fully exploited in the proof-of-concept microfluidic fuel cell, primarily due to its high parasitic ohmic resistance. While electrode contamination from the carbonate species is a possibility at high fuel concentrations, no detectable deterioration was observed in these tests.

Finally, we also assembled a prototype microfluidic fuel cell with a Pd cathode, to evaluate the performance gains compared to the cell with a Au cathode, envisaged by the *ex situ* measurements. The cell generated an initial peak power density of 59 mW cm^{-2} (at a flow rate of 60 μL min^{-1}), 13% higher than the previous cell, but the gas bubbles growing on the Pd cathode made its operation unstable shortly thereafter. To enable reliable fuel cell operation with a Pd cathode, some design modifications need to be undertaken. Potentially a grooved channel geometry for gas removal could be incorporated, as previously demonstrated [13]. An alternative strategy is to evaluate other catalysts for the hypochlorite reduction that do not produce gas. Both platinum [27] and a combination of palladium and iridium [28] have been used effectively for hypochlorite reduction but their application in microfluidic fuel cells needs to be assessed.

4. Conclusions

This work demonstrated the feasibility of an alkaline formate anode coupled with an alkaline hypochlorite cathode in a microfluidic fuel cell architecture with flow-through porous electrodes. Both half-cells were unique in terms of fuel cell implementation. In contrast to the vanadium redox system, formate and hypochlorite are both available in highly concentrated solutions, thereby enabling a microfluidic fuel cell system with high overall energy density. The proof-of-concept formate/hypochlorite microfluidic fuel cell concurrently achieved high power densities and near-complete fuel utilization at relatively high cell voltages, and therefore enabled high overall energy conversion efficiency. The performance would be enhanced further by reducing the combined ohmic resistance of the cell, specifically the on-chip electrical contact resistance, and by performing a catalyst screening study for hypochlorite reduction to reduce the activation overpotential and enhance the electrochemical kinetics while preventing gas evolution. Other advancements under investigation include employing higher fuel and oxidant concentrations in the fuel cell, switching to potassium hydroxide electrolyte and optimizing its concentration, and evaluating other liquid hydrocarbon fuels such as methanol. The new alkaline formate and hypochlorite fuel cell concept demonstrated here, or either one of its individual half-cells, may also find applications using conventional membrane-based fuel cell designs.

Acknowledgments

The authors would like to acknowledge project funding by the Natural Sciences and Engineering Research Council of Canada (NSERC) and Angstrom Power Inc., and infrastructure funding from Canada Foundation for Innovation (CFI) and British Columbia Knowledge Development Fund (BCKDF).

References

[1] A. Bazylak, D. Sinton, N. Djilali, Journal of Power Sources 143 (2005) 57.
[2] M.H. Chang, F. Chen, N.S. Fang, Journal of Power Sources 159 (2006) 810.
[3] F.L. Chen, M.H. Chang, M.K. Lin, Electrochimica Acta 52 (2007) 2506.
[4] E.R. Choban, L.J. Markoski, A. Wieckowski, P.J.A. Kenis, Journal of Power Sources 128 (2004) 54.
[5] E.R. Choban, J.S. Spendelow, L. Gancs, A. Wieckowski, P.J.A. Kenis, Electrochimica Acta 50 (2005) 5390.
[6] E.R. Choban, P. Waszczuk, P.J.A. Kenis, Electrochemical and Solid State Letters 8 (2005) A348.
[7] J.L. Cohen, D.J. Volpe, D.A. Westly, A. Pechenik, H.D. Abruna, Langmuir 21 (2005) 3544.
[8] J.L. Cohen, D.A. Westly, A. Pechenik, H.D. Abruna, Journal of Power Sources 139 (2005) 96.
[9] R. Ferrigno, A.D. Stroock, T.D. Clark, M. Mayer, G.M. Whitesides, Journal of the American Chemical Society 124 (2002) 12930.
[10] S. Hasegawa, K. Shimotani, K. Kishi, H. Watanabe, Electrochemical and Solid State Letters 8 (2005) A119.
[11] R.S. Jayashree, D. Egas, J.S. Spendelow, D. Natarajan, L.J. Markoski, P.J.A. Kenis, Electrochemical and Solid State Letters 9 (2006) A252.
[12] R.S. Jayashree, L. Gancs, E.R. Choban, A. Primak, D. Natarajan, L.J. Markoski, P.J.A. Kenis, Journal of the American Chemical Society 127 (2005) 16758.
[13] E. Kjeang, A.G. Brolo, D.A. Harrington, N. Djilali, D. Sinton, Journal of the Electrochemical Society 154 (2007) B1220.
[14] E. Kjeang, J. McKechnie, D. Sinton, N. Djilali, Journal of Power Sources 168 (2007) 379.
[15] E. Kjeang, R. Michel, D.A. Harrington, N. Djilali, D. Sinton, Journal of the American Chemical Society 130 (2008) 4000.
[16] E. Kjeang, B.T. Proctor, A.G. Brolo, D.A. Harrington, N. Djilali, D. Sinton, Electrochimica Acta 52 (2007) 4942.
[17] E. Kjeang, D. Sinton, D.A. Harrington, Journal of Power Sources 158 (2006) 1.
[18] S.M. Mitrovski, L.C.C. Elliott, R.G. Nuzzo, Langmuir 20 (2004) 6974.
[19] S.M. Mitrovski, R.G. Nuzzo, Lab on a Chip 6 (2006) 353.
[20] K.G. Lim, G.T.R. Palmore, Biosensors & Bioelectronics 22 (2007) 941.
[21] C.M. Moore, S.D. Minteer, R.S. Martin, Lab on a Chip 5 (2005) 218.
[22] M. Togo, A. Takamura, T. Asai, H. Kaji, M. Nishizawa, Electrochimica Acta 52 (2007) 4669.
[23] A. Kundu, J.H. Jang, J.H. Gil, C.R. Jung, H.R. Lee, S.H. Kim, B. Ku, Y.S. Oh, Journal of Power Sources 170 (2007) 67.
[24] J.D. Morse, International Journal of Energy Research 31 (2007) 576.
[25] Y.M. Zhu, Z. Khan, R.I. Masel, Journal of Power Sources 139 (2005) 15.
[26] S. Licht, Electrochemistry Communications 1 (1999) 33.
[27] A.M. Cardenas-Valencia, C.J. Biver, L. Langebrake, Journal of Power Sources 166 (2007) 273.
[28] M.G. Medeiros, E.G. Dow, Journal of Power Sources 80 (1999) 78.
[29] S.J. You, Q.L. Zhao, J.N. Zhang, J.Q. Jiang, S.Q. Zhao, Journal of Power Sources 162 (2006) 1409.
[30] J.J. Whalen, J.D. Weiland, P.C. Searson, Journal of the Electrochemical Society 152 (2005) C738.
[31] D.D. Wagman, W.H. Evans, V.B. Parker, R.H. Schumm, I. Halow, S.M. Bailey, K.L. Churney, R.L. Nuttall, Journal of Physical and Chemical Reference Data 11 (Suppl. (2)) (1982).
[32] D.R. Lide, CRC Handbook of Chemistry and Physics, CRC Press, Boca Raton, FL, 2002.